Available online at www.sciencedirect.com
ScienceDirect
Journal of Environmental Sciences 2011, 23(2) 199–205
JOURNAL OF ENVIRONMENTAL SCIENCES
ISSN 1001-0742
CN 11-2629/X
www.jesc.ac.cn

Removal of phosphate by Fe-coordinated amino-functionalized 3D mesoporous silicates hybrid materials

Jianda Zhang[1], Zhemin Shen[1], Zhijian Mei[1], Shanping Li[2], Wenhua Wang[1,*]

1. School of Environmental Science and Engineering, Shanghai Jiaotong University, Shanghai 200240, China. E-mail: zjdrf@163.com
2. School of Environmental Science and Engineering, Shandong University, Jinan 250100, China

Received 29 January 2010; revised 23 April 2010; accepted 28 April 2010

Abstract

Phosphate removal from aqueous waste streams is an important approach to control the eutrophication downstream bodies of water. A Fe(III) coordinated amino-functionalized silicate adsorbent for phosphate adsorption was synthesized by a post-grafting and metal cation incorporation process. The surface structure of the adsorbent was characterized by X-ray diffraction, N_2 adsoropion/desoprotion technique, and Fourier transform infrared spectroscopy. The experimental results showed that the adsorption equilibrium data were well fitted to the Langmuir equation. The maximum adsorption capacity of the modified silicate material was 51.8 mg/g. The kinetic data from the adsorption of phosphate were fitted to pseudo second-order model. The phosphate adsorption was highly pH dependent and the relatively high removal of phosphate fell within the pH range 3.0–6.0. The coexistence of other anions in solutions has an adverse effect on phosphate adsorption; a decrease in adsorption capacity followed the order of exogenous anions: $F^- > SO_4^{2-} > NO_3^- > Cl^-$. In addition, the adsorbed phosphate could be desorbed by NaOH solutions. This silicate adsorbent with a large adsorption capacity and relatively high selectivity could be utilized for the removal of phosphate from aqueous waste streams or in aquatic environment.

Key words: phosphate; mesoporous material; Fe coordinated; adsorption

DOI: 10.1016/S1001-0742(10)60393-2

Citation: Zhang J D, Shen Z M, Mei Z J, Li S P, Wang W H, 2011. Removal of phosphate by Fe-coordinated amino-functionalized 3D mesoporous silicates hybrid materials. Journal of Environmental Sciences, 23(2): 199–205

Introduction

Wastewater from municipal, industrial and agricultural activities usually contains considerable amounts of dissolved phosphate, and its discharge to receiving bodies of water often causes eutrophication (De Vicente et al., 2008; Jalali and Kolahchi, 2009). In order to prevent eutrophication, strict discharge standards of phosphate (e.g., < 0.5–1.0 mg P/L) must be applied to waste streams to control the level of phosphate in water (Ugurlu and Salman, 1998). Currently, the treatment technologies applied to phosphate removal mainly include biological removal (Mulkerrins et al., 2004), chemical precipitation (Yigit and Mazlum, 2007), crystallization (Kim et al., 2006), ion exchange (Chen et al., 2002), and adsorption (Guan et al., 2007).

However, phosphorus is an important nonrenewable natural resource. Worldwide, the available phosphorus is estimated to meet human demand for only around one century (Driver et al., 1999). Therefore, it is worthwhile to seek feasible technologies to capture, recover and reuse this potentially limited resource. In current phosphate removal approaches, chemical technologies can recover the phosphate from wastewater, but at increased cost due to the large amount of chemical waste resulting from the process. Recently, some researchers have paid attention to adsorption techniques that not only be applied for phosphate removal, but also for phosphate recovery. Various materials have been studied as phosphate adsorbents including dolomite (Ayoub and Kalinian, 2006), zeolites (Ning et al., 2008), blast furnace slag (Hedstrom and Rastas, 2006), banana stems (Anirudhan et al., 2006) and tree bark (Tshabalala et al., 2004).

MCM-41 is a mesoporous molecular sieve because of its sharp and ordered pore distribution, high surface area and large pore volume (Kresge et al., 2004), MCM-41 has been used widely as an adsorbent and catalyzer support. Studies have revealed that the irons are effective for phosphate adsorption based on cation-anion interaction and Fe can be coordinated by amino group. In addition, the cost of Fe is low. Therefore, it is feasible and practical to prepare a new phosphate adsorbent combined with each advantage. In this article, a Fe(III) loaded silicate material was prepared by incorporated Fe(III) to an amino-functionalized MCM-41 that synthesized by a post-grafting method. The adsorbent material and its phosphate adsorption behavior was characterized; the effects

* Corresponding author. E-mail: wangwh@sjtu.edu.cn

of adsorbent dose, temperature, solution pH, contact time, the coexistence of competitive ions and initial phosphate concentration on phosphate adsorption were evaluated by batch experiments. In addition, adsorption isotherms and the kinetics of phosphate adsorption on adsorbent were investigated.

1 Materials and methods

1.1 Reagents

KH_2PO_4, NaOH, HCl, tetra ethyl ortho silicate (TEOS), and hexadecyl trimethyl ammonium bromide (CTAB) were of analytical grade and obtained from Shanghai Chemical Co., China. Stock solutions of phosphate were prepared by using anhydrous KH_2PO_4.

1.2 Synthesis of adsorbent

MCM-41 was synthesized according to the procedure described elsewhere by a templating method (Zhao et al., 2000). TEOS was used as organic Si source and CTAB used as template. CTAB of 2.4 g was added into the mixture of 40 g distilled water and 2.15 g NaOH. Then, 5 mL TEOS was added slowly into the mixture until the solution became a clear gel. The mixture was stirred for 2 hr and transferred into PTFE-lined autoclave under autogenous pressure at 110°C for 48 hr. The white solid product was washed, filtered, dried, and calcined at 550°C with the heat rate of 1°C/min. The amino-functionalized silicate material denoted as NN-M41 was prepared via the post-synthesis grafting method according to Yokoi et al. (2004). Specifically, 5 g of calcined MCM-41 was stirred with 15 mL 1-(2-aminoethyl)-3-aminopropyltrimethxoysilane (Momentive Performance Materials, Inc., USA) in dry toluene. The mixture was heated at 110°C under an inert atmosphere for 6 hr. The amino-functionalized material was purified by filtration, washed with 2-propanol, and dried at 100°C, resulting in a white powder. The Fe(III)-coordinated silicate material, "Fe-NN-MCM-41", was prepared by stirring an excess amount of Fe(III) chlorate hexahydrate in 2-propanol solution with NN-M41 for 2 hr at 25°C. The resulting yellowy powder was collected by filtration, washed with 2-propanol and dried at 100°C.

1.3 Characterization

Powder X-ray diffraction (XRD) patterns of each samples were recorded on a diffractometer (D/max-2200/PC, Rigaku Corporation, Japan) using Cu K_α radiation at 40.0 kV and 30.0 mA in the 2θ range of 0.8°–8° with a scan speed of 1°/min. The pore structures distribution and BET area of the samples were measured at 77 K with an N_2 physical adsorption/desorption technique using a surface area and porosimetry analyzer (ASAP 2010 M+C, Micromeritics, Inc., USA). Prior to analysis, the pure MCM-41 was degassed at 200°C for 6 hr under vacuum; the functionalized materials were degassed at 120°C for 12 hr under vacuum. Fourier transform infrared spectroscopy (FT-IR) spectra of solid samples were obtained using a Shimadzu IRPrestige-21 instrument (Japan) with 2 cm^{-1} resolution between 200 and 4000 cm^{-1}. Separate KBr pellets containing approximately 0.5% of each sample was prepared for the FT-IR analysis. Carbon and nitrogen were determined with an elemental analyzer (Vario EL III, Elementar Corporation, USA). The amino group content of the functionalized mesoporous silica was calculated based on the determined nitrogen content. The Fe content was determined by inductively coupled plasma (ICP) (Iris Advantage 1000, Thermo Corporation, USA).

1.4 General procedure for batch phosphate adsorption experiments

Batch adsorption tests were carried out to determine the adsorption behavior of phosphate with Fe-NN-M41. The specific parameters investigated were adsorption equilibrium isotherms, adsorption kinetics, pH dependency, and the effect of competition from coexisting anions coexist anions. Equilibrium experiments were initially carried out at varied phosphate concentrations at a constant pH 7.0. Replicate mixtures consisting of 0.100 g adsorbent were mixed with 100 mL phosphate solution at various initial concentrations in 250 mL glass-stoppered conical flasks. The initial pH of the phosphate working solution was adjusted to 7.0 by 0.1 mol/L NaOH and 0.1 mol/L HCl. The sealed flasks were then placed in an thermostatted air bath rotary shaker (HZQ-F, Harbin Donglian Electronic & Technology Development Co., Ltd., China) maintained at 25, 35, 45°C, and shaken at 120 r/min for 4 hr to attain equilibrium. The suspension was then filtered with a 0.45-μm membrane syringe filter. The remaining phosphate concentration of the filtered solution was analyzed using the ascorbic acid method by monitoring the absorbance at 880 nm on spectrophotometer (Unico UV-2102 PCS, Unico Corp., China; APHA, 1985). The sorption amount of phosphate at equilibrium, q_e (mg/g), can be calculated by:

$$q_e = \frac{(C_0 - C_e)V}{m} \quad (1)$$

where, C_0 (mg/L) and C_e (mg/L) are the initial and equilibrium liquid phase phosphate concentrations, respectively, V (L) is the volume of the solution and m (g) is the mass of the adsorbent. All experiments were replicated twice and mean values were reported.

Adsorption kinetic experiments were performed as follows: 0.100 g adsorbent was added into 100 mL phosphate working solutions (30, 50, or 100 mg/L). The solution pH was adjusted to 7.0. The sealed conical flasks were transferred to a shaker bath at 25°C, and shaken at 120 r/min. The phosphate concentration was measured at 0, 2, 5, 10, 30, 60, 120, and 240 min. The effect of pH on phosphate adsorption was examined in series of batch experiments at different pH values ranging from 2.0 to 12.0. An initial phosphate concentration was 100 mg/L and 1.00 g of adsorbent per liter of solution was added. The effect of coexisting anions on adsorption of phosphate was evaluated by having the sodium salt forms of F^-, Cl^-, NO_3^-, and SO_4^{2-} (at 100, 300, 500, 700, or 900 mg/L) present in

the phosphate solutions. Initial phosphate concentration of 50 mg/L and 1.00 g adsorbent per liter of solution were used and the initial pH of final combined solution was adjusted to 7.0.

1.5 Desorption kinetic study

Each adsorbents used above for the initial studies of adsorption was collected by filtration from the above batch experiments using a 0.45-μm syringe filter. The spent adsorbent was then mixed with 100 mL of 0.01 mol/L NaOH solution, and evaluated for phosphate concentration using aliquots taken out at a regular time interval.

2 Results and discussion

2.1 X-ray diffraction

The structures of MCM-41, NN-M41 and Fe-NN-M41 were determined by solid state, low angel X-ray diffraction. The results are illustrated in Fig. 1. The diffraction patterns of MCM-41 exhibited significant peaks for the (100), (110), and (200) reflections, which is characteristic of mesoporous materials with long-range hexagonal arrays. In contrast, the intensity reduction of the XRD patterns of NN-M41 and Fe-NN-M41were observed. In these materials, the (110) and (200) peaks of the modified samples decrease dramatically. The remarkable change in the (100) peak and disappearance of (110) and (200) peaks of the modified samples suggests the structural degradation of the post-synthesis functionalized materials. Similar results have been reported previously (Rivera-Jimenez and Hernandez-Maldonado, 2008); the observed change in XRD patterns may be due to the collapse of the long-range ordered structure of MCM-41 due to the process of grafting on organic amino group.

2.2 N_2 adsorption/desorption isotherms

Nitrogen adsorption/desorption isotherms are illustrated in Fig. 2. The isotherm can be classified as type IV according to IUPAC classification standard. The isotherm curves feature linear to step-shaped uptakes at partial pressure between 0.1 and 0.8. Table 1 summarizes the results of nitrogen adsorption experiments for MCM-41,

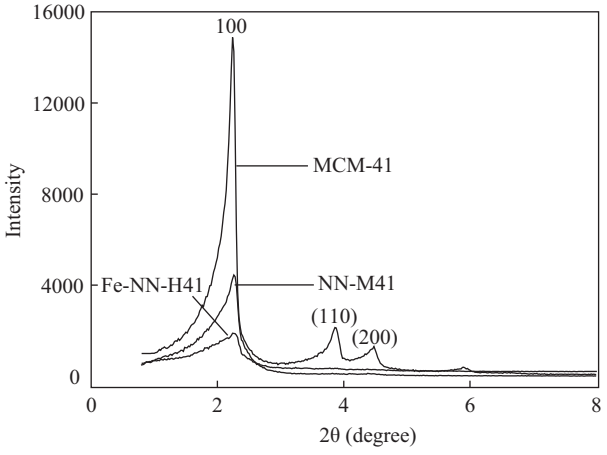

Fig. 1 X-ray diffraction patterns of MCM-41, NN-M41 and Fe-NN-M41.

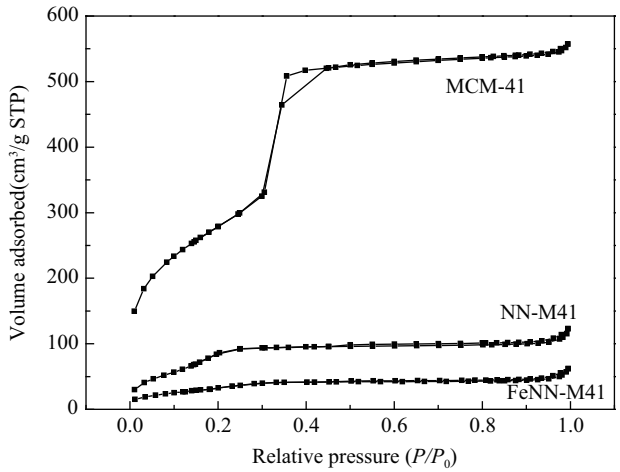

Fig. 2 Nitrogen adsorption-desorption isotherms of MCM-41, NN-M41 and Fe-NN-M41. STP: standard temperature and pressure.

NN-M41, and Fe-NN-M41. For MCM-41, the BET surface area and average pore diameter are 1015 m^2/g and 3.09 nm, respectively. After grafting the amino group into the framework wall of MCM-41, there is a large decrease in the surface area, pore volume, and pore size. The structure parameter changes are due to the occupation of surface organic groups in the mesopore channels of MCM-41 (Mercier and Pinnavaia, 1998; Brown et al., 2000). In addition, the coordination of Fe(III) caused smaller reduction of the BET surface area and pore volume, again due to the occupation of volume within the mesoporous volume of the material.

Table 1 Summary of the porosimetry data for MCM-41, NN-M41 and Fe-NN-M41

Sample	BET surface area (m^2/g)	Pore diameter (nm)	Total pore volume (cm^3/g)
MCM-41	1015	3.09	0.86
NN-M41	348	2.82	0.19
Fe-NN-M41	145	2.62	0.11

2.3 FT-IR

Infrared spectroscopy was used to monitor the changes in the surface of silica-based samples. IR bands related to the MCM-41 and to the grafted amino groups are shown in

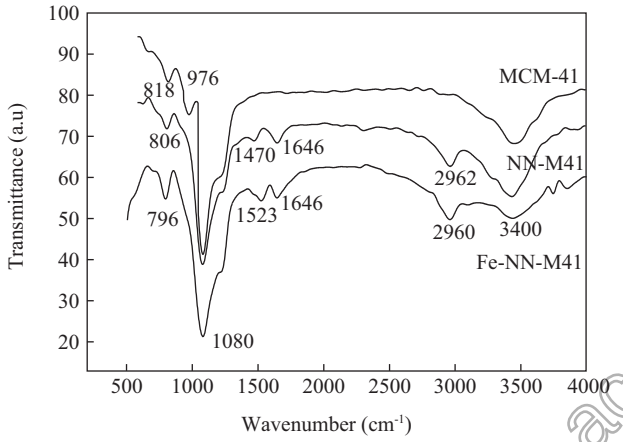

Fig. 3 IR spectra of MCM-41, NN-MCM-41; Fe-NN-MCM-41.

Fig. 3. The bands at 1080, 818, and 976 cm^{-1} corresponded to the Si–O–Si asymmetric, Si–O–Si symmetric vibrations, and Si–OH vibrations, respectively. The broad band around 3400 in the hydroxyl region illustrates the presence of silanol groups within the MCM-41 pore channel. For NN–M41, amino-functionalized materials, weak bands appear at 1470 and 1646 cm^{-1} due to NH_2 vibrations. The feature near at 2900–3000 cm^{-1} corresponds to the vibrations of the alkyl C–H group. Band at 976 cm^{-1} disappears after grafting procedure, which is expected due to the reaction of the MCM-41 surface –Si–OH groups with –Si–O–CH_3. Elemental analysis indicated that the C and N content was 13.21% and 5.01%, respectively, which well matched the molecular formula $C_5N_2H_{13}$. Similar results are reported by other researchers for amino-modified MCM-41 materials (Diaz et al., 1997; Rivera-Jimenez and Hernandez-Maldonado, 2008). The Fe content in Fe-NN-M41 determined was 3.64%.

2.4 Adsorption isotherm models

Isotherm studies under 25, 35 and 45°C were performed to determine the maximum adsorption capacity of phosphate on Fe-NN-M41. The plot of phosphate adsorption capacity against the phosphate equilibrium concentration is shown in Fig. 4. Langmuir and Freundlich equations were applied to describe the adsorption isotherm.

Langmuir equation:

$$\frac{C_e}{q_e} = \frac{1}{q_0 K_L} + \frac{C_e}{q_0} \quad (2)$$

where, C_e (mg/L) is the concentration of phosphate solution at equilibrium, q_e (mg/g) is the amount of the phosphate absorbed by per unit of the adsorbent, and q_0 (mg/g) and K_L (L/mg) are Langmuir constants related to the adsorption capacity and energy of adsorption for a sorbent material, respectively.

Freundlich equation:

$$\log q_e = \log K_F + \frac{1}{n} \log C_e \quad (3)$$

where, K_F (mg/g) and n are the constants of a Freundlich isotherm that measure the adsorption capacity and intensity of adsorption, respectively.

The isotherm data were applied to the Langmuir and Freundlich models by non-linear regression using the method of least squares with Origin 7.0. The estimated adsorption constants with corresponding correlation coefficients (R^2) are summarized in Table 2. The value of correlation coefficients obtained for each model indicates the Langmuir model provides a better fit than

Table 2 Langmuir and Freundlich isotherms constants

Temperature (°C)	Langmuir equation			Freundlich equation		
	Q (mg/g)	K_L (L/mg)	R^2	n	K_F (mg/g)	R^2
25	51.8	0.0624	0.999	4.62	15.08	0.876
35	50.8	0.0411	0.998	3.71	10.70	0.880
45	44.8	0.0138	0.955	2.89	6.01	0.799

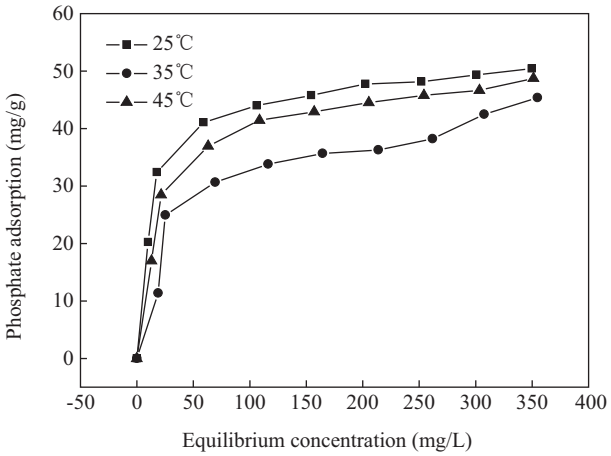

Fig. 4 Adsorption isotherm of phosphate by Fe-NN-M41. Adsorbent dose: 0.100 g/100 mL; pH: 7; stirring speed: 120 r/min.

the Freundlich model. The Langmuir equation assumes that the adsorption occurs on a homogeneous surface, which suggests that the Fe incorporated into NN-M41 maintains a relatively homogenous surface. In contrast, the Freundlich equation describes adsorption on adsorbent with heterogeneous surfaces. The maximum adsorption capacity calculated using Langmuir model is 51.8, 50.8 and 44.8 mg/g respectively, at 25, 35 and 45°C. Comparing with other reported data, Fe-NN-M41 possesses a higher adsorption capacity for phosphate than La-modified zeolite (24.6 mg/g), La-drop vesuvianite (20.5 mg/g) and mesoporous ZrO_2 (29.7 mg/g) (Ning et al., 2008; Li et al., 2009; Liu et al., 2008). The results indicate the Fe-NN-M41 reported here possesses superior phosphate adsorption capability.

2.5 Adsorption kinetic studies

Adsorption kinetic experiments were conducted to determine the rate of phosphate adsorption on Fe-NN-M41 using initial phosphate concentrations of 30, 50, 100 mg/L. Figure 5 illustrates the adsorption of phosphate against

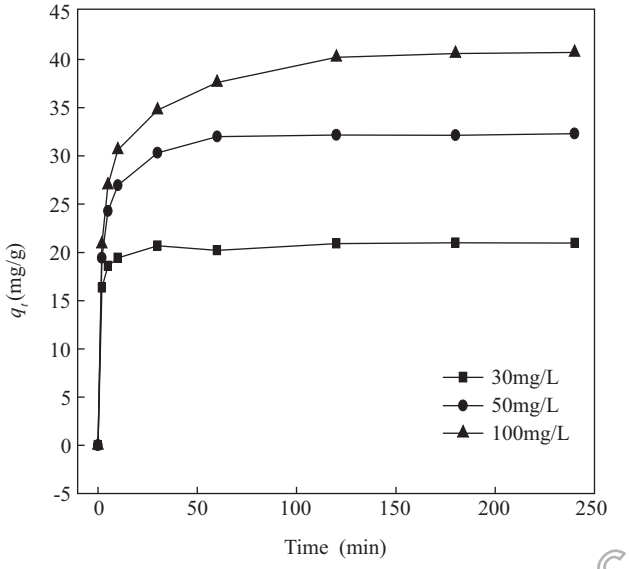

Fig. 5 Effect of contact time and initial concentration on the phosphate adsorption onto Fe-NN-M41. Adsorbent dose: 0.100g/100 mL; temperature: 25°C; pH 7; stirring speed: 120 r/min.

contact time, and all three curves exhibit the same trend. The adsorption of phosphate increases as expected over the time course of the experiment and reached saturation after 240 min, and the adsorption of phosphate increased with increasing initial concentration. At initial concentration 30 mg/L, the adsorption process could be separated into three steps. In the first step (0–5 min), the adsorption rate was quick and about 90.3% of the final adsorption capacity could be accomplished. This may be due to the fine particles of MCM-41 and high dispersal of Fe ions. In addition, the concentration gradient between solution bulk and surface of Fe-NN-M41 were also contributed to the high adsorption rate. In the second step (5–60 min), the adsorption rate became slow and the intraparticle diffusion dominated in this process. After 60 min, the adsorption capacity did not change and the adsorption process reached equilibrium. To evaluate the adsorption kinetic process, the phosphate adsorption kinetic data were analyzed using pseudo first and second-order models by non-linear regression. The kinetic equations for these models are as follows (Lagergren, 1898; Blanchard et al., 1984):

$$\log(q_e - q_t) = \log q_e - k_1 t/2.303 \quad (4)$$

$$\frac{t}{q_t} = \frac{1}{k_2 q_e^2} + \frac{t}{q_e} \quad (5)$$

The rate constants of pseudo second-order model are presented in Table 3. The high value of correlation coefficient ($R^2 > 0.99$) illustrate that the kinetic data fitted well with the pseudo second-order model suggesting that the adsorption process might be chemisorption. The correlation coefficient of pseudo first-order is so poor that the rate constants are not shown in Table 3.

Table 3 Kinetic parameters for phosphate adsorption on Fe-NN-M41

Initial concentration (mg/L)	q_e (exp) (mg/g)	Second-order kinetics parameter		
		k_2 (g/(mg·min))	q_e (cal) (mg/g)	R^2
30	20.9	0.065	21.0	0.999
50	32.3	0.019	32.9	0.999
100	40.7	0.008	41.2	0.999

2.6 Influence of initial pH on adsorption of phosphate

Initial pH is usually considered to influence the adsorption of anions at the solid-liquid interfaces in aqueous systems. The adsorption of phosphate on Fe-NN-M41 was investigated at pH values ranging from 2.0 to 12.0 starting with an initial phosphate concentration of 50 mg/L, adsorbent dose of 1.00 g/L, and temperature of 25°C. As shown in Fig. 6, it is obvious that phosphate adsorption onto Fe-NN-M41 strongly pH dependent. There are two prominent points in the measured adsorption at pH 3.0 and 6.0. The adsorption of phosphate remains at a maximum level within this pH range, and deceases dramatically beyond this pH range. A similar result was also observed by other researchers investigating phosphate adsorption on $ZnCl_2$-activated coir pith carbon (Namasivayam and Sangeetha, 2004). The observed trend is related to phosphate proton dissociation equilibria. Phosphate can exist

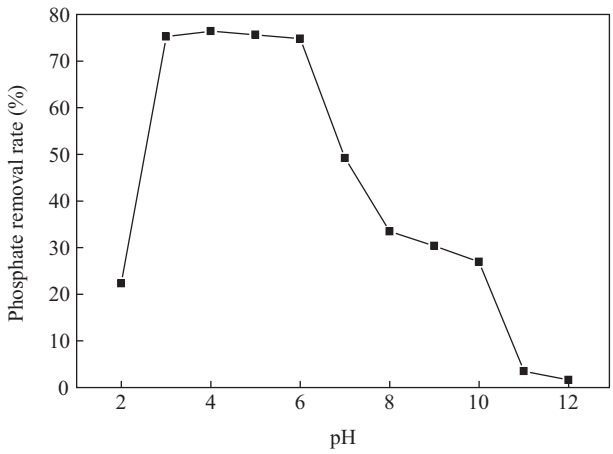

Fig. 6 Effect of pH on adsorption of phosphate. Adsorption dose: 0.100 g/100 mL; initial phosphate concentrations: 50 mg/L; agitation time: 240 min; temperature: 25°C.

as of H_3PO_4, $H_2PO_4^-$, HPO_4^{2-} and PO_4^{3-}, depending on the solution pH value. Below pH 3.0, the predominant species is H_3PO_4, which is weakly attached bound to adsorbent sites. With the increase in solution pH, the dominant species are $H_2PO_4^-$ and HPO_4^{2-} which readily adsorbed by the Fe(III) sites on the adsorbent by electrostatic interactions. The higher pH not only causes the adsorbent surface to carry more negative charges, but also leads to a high concentration of hydroxide groups. Therefore, there may also be increased competition between negatively charged phosphate species and hydroxide groups on more negatively charged adsorbent surface sites to causes the lower adsorption of phosphate at higher pH.

2.7 Effect of coexisting anions on adsorption capacity

Phosphate adsorption on Fe-NN-M41 was separately investigated in the presence of following competing anions: F^-, Cl^-, NO_3^-, and SO_4^{2-}. As shown in Fig. 7, a decrease in phosphate removal was observed when the concentration of competitive ions was increased from 0 to 900 mg/L. The four competing anions had different adverse effect on phosphate removal. The inhibition on phosphate adsorption follows the order: $SO_4^{2-} > F^- >$

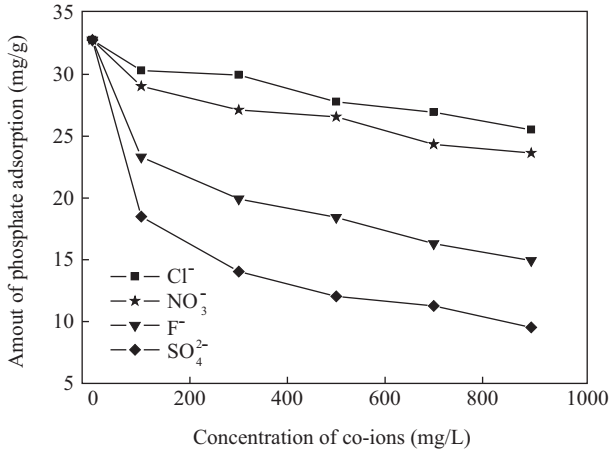

Fig. 7 Effect of coexisting anions on adsorption capacity. Adsorbent dose: 0.100 g/100 mL; phosphate concentration: 50 mg/L; foreign anions concentrations: 400 mg/L; pH 7; temperature: 25°C; stirring speed: 120 r/min.

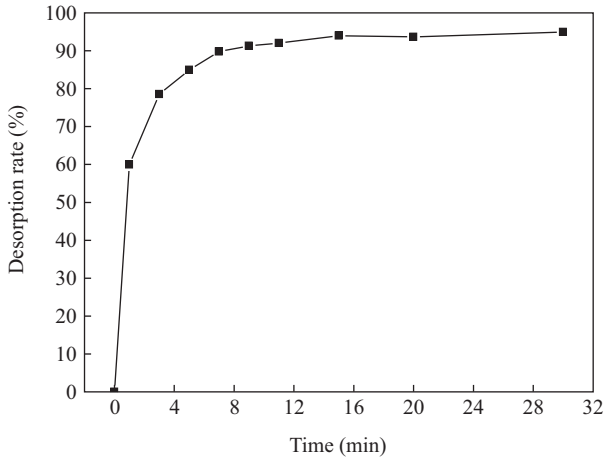

Fig. 8 Desorption kinetics of phosphate at 25°C in 0.01 mol/L NaOH solution. Adsorbent dose: 0.100 g/100 mL; stirring speed: 120 r/min; temperature: 25°C.

$Cl^- > NO_3^-$. Among the four anions, SO_4^{2-} has largest impact on the adsorption of phosphate by Fe-NN-M41. In this case, phosphate adsorption decreased three-fold, from 32.8 to 9.5 mg/L. An ion exchange reaction may be proposed as a mechanism for phosphate adsorption in this material, specifically, an exchange occurs between phosphate ions and the hydroxide ions at the Fe(III) site. Thus, the decrease in the adsorption capacity may be explained on the basis of ion exchange mechanism where sulfate possesses the highest affinity for the adsorbent material and competes most effectively against phosphate adsorption. The order of the effect of the other anions on the phosphate adsorption may also be related to affinity of the anions toward the adsorbent.

2.8 Desorption study

To recover adsorbed phosphate, 0.01 mol/L NaOH was used to treat the spent adsorbents. The desorption of the spent adsorbents is shown in Fig. 8. Under the alkaline conditions, the desorption is rapid and almost complete within 30 min, indicating the reversible adsorption of phosphate on the Fe-NN-M41 material. More than 90% of the adsorbed phosphate was desorbed into 0.01 mol/L NaOH solution. There results suggested the Fe-NN-M41 has the potential to recover the adsorbed phosphate.

3 Conclusions

A novel iron-containing silicate material for phosphate adsorption, Fe-NN-M41, was obtained by post-grafting MCM-41 and incorporation of Fe(III) as the chlorate salt. The silica samples were characterized by XRD, N_2 adsorption/desorption, and FT-IR. Phosphate adsorption fit well to Langmuir isotherms and the maximum phosphate adsorption for Fe-NN-M41 was found to be 51.8 mg/g at 25°C. Kinetic data were fit to a pseudo second-order model. Maximal phosphate adsorption was achieved within the pH range of 3.0 to 6.0. The presence of exogenous competitive ions in solution decreased the phosphate adsorption capacity and followed the order of $SO_4^{2-} > F^- > Cl^- > NO_3^-$. Adsorbed phosphate can be effectively desorbed by a 0.01 mol/L NaOH solution. The Fe-NN-M41 material, with a high adsorption capacity and relatively high selectively, may have applications as an adsorbent for the removal of phosphate ions from waste streams or in the treatment of contaminated bodies of water.

Acknowledgments

This work was supported by the National Major Research Plan for Water Pollution Control and Treatment of China (No. 2009ZX07101-015, 2009ZX07105-003). We also want to thank Dr. David for his valuable work on our manuscript revision.

References

Anirudhan T S, Noeline B F, Mancihar D M, 2006. Phosphate removal from wastewaters using a weak anion exchanger prepared from a lignocellulosic residue. *Environmental Science & Technology*, 40(8): 2740–2745.

APHA (American Public Health Association), 1985. Standard Methods for the Examination of Water and Wastewater (16th ed.). Washington DC, USA.

Ayoub G M, Kalinian H, 2006. Removal of low-concentration phosphorus using a fluidized raw dolomite bed. *Water Environment Research*, 78(4): 353–361.

Brown J, Richer R, Mercier L, 2000. One-step synthesis of high capacity mesoporous Hg^{2+} adsorbents by non-ionic surfactant assembly. *Microporous and Mesoporous Materials*, 37(1-2): 41–48.

Chen J P, Chua M L, Zhang B P, 2002. Effects of competitive ions, humic acid, and pH on removal of ammonium and phosphorous from the synthetic industrial effluent by ion exchange resins. *Waste Management*, 22(7): 711–719.

De Vicente I, Jensen H S, Andersen F O, 2008. Factors affecting phosphate adsorption to aluminum in lake water: Implications for lake restoration. *Science of the Total Environment*, 389(1): 29–36.

Diaz J F, Balkus K J, Bedioui F, Kurshev V, Kevan L, 1997. Synthesis and characterization of cobalt-complex functionalized MCM-41. *Chemistry of Materials*, 9(1): 61–67.

Driver J, Lijmbach D, Steen I, 1999. Why recover phosphorus for recycling, and how? *Environmental Technology*, 20(7): 651–662.

Blanchard G, Maunaye M, Martin G, 1984. Removal of heavy metals from waters by means of natural zeolites. *Water Research*, 18(12): 1501–1507.

Guan X H, Chen G H, Shang C, 2007. Adsorption behavior of condensed phosphate on aluminum hydroxide. *Journal of Environmental Sciences*, 19(3): 312–318.

Hedstrom A, Rastas L, 2006. Methodological aspects of using blast furnace slag for wastewater phosphorus removal. *Journal of Environmental Engineering-Asce*, 132(11): 1431–1438.

Jalali M, Kolahchi Z, 2009. Effect of irrigation water quality on the leaching and desorption of phosphorous from soil. *Soil & Sediment Contamination*, 18(5): 576–589.

Kim E H, Yim S B, Jung H C, Lee E J, 2006. Hydroxyapatite crystallization from a highly concentrated phosphate solution using powdered converter slag as a seed material. *Journal of Hazardous Materials*, 136(3): 690–697.

Kresge C T, Vartuli J C, Roth W J, Leonowicz M E, 2004. The discovery of ExxonMobil's M41S family of mesoporous

molecular sieves. *Mesoporous Crystals and Related Nano-Structured Materials*, 148: 53–72.

Li H, Ru J Y, Yin W, Liu X H, Wang J Q, Zhang W D, 2009. Removal of phosphate from polluted water by lanthanum doped vesuvianite. *Journal of Hazardous Materials*, 168(1): 326–330.

Liu H L, Sun X F, Yin C G, Hu C, 2008. Removal of phosphate by mesoporous ZrO_2. *Journal of Hazardous Materials*, 151(2-3): 616–622.

Mercier L, Pinnavaia T J, 1998. Heavy metal lan adsorbents formed by the grafting of a thiol functionality to mesoporous silica molecular sieves: Factors affecting Hg(II) uptake. *Environmental Science & Technology*, 32(18): 2749–2754.

Mulkerrins D, Dobson A D W, Colleran E, 2004. Parameters affecting biological phosphate removal from wastewaters. *Environment International*, 30(2): 249–259.

Namasivayam C, Sangeetha D, 2004. Equilibrium and kinetic studies of adsorption of phosphate onto $ZnCl_2$ activated coir pith carbon. *Journal of Colloid and Interface Science*, 280(2): 359–365.

Ning P, Bart H J, Bing L, Lu X W, Zhang Y, 2008. Phosphate removal from wastewater by model-La(III) zeolite adsorbents. *Journal of Environmental Sciences*, 20(6): 670–674.

Rivera-Jimenez S M, Hernandez-Maldonado A J, 2008. Nickel(II) grafted MCM-41: A novel sorbent for the removal of Naproxen from water. *Microporous and Mesoporous Materials*, 116(1-3): 246–252.

Lagergren S, 1898. Zur theorie der sogenannten adsorption gelöster stoffe. *Kungliga Svenska Vetenskapsakademiens, Handlingar*, 24(4): 1–39.

Tshabalala M A, Karthikeyan K G, Wang D, 2004. Cationized milled pine bark as an adsorbent for orthophosphate anions. *Journal of Applied Polymer Science*, 93(4): 1577–1583.

Ugurlu A, Salman B, 1998. Phosphorus removal by fly ash. *Environment International*, 24(8): 911–918.

Yigit N O, Mazlum S, 2007. Phosphate recovery potential from wastewater by chemical precipitation at batch conditions. *Environmental Technology*, 28(1): 83–93.

Yokoi T, Yoshitake H, Tatsumi T, 2004. Synthesis of amino-functionalized MCM-41 via direct co-condensation and post-synthesis grafting methods using mono-, di- and tri-amino-organoalkoxysilanes. *Journal of Materials Chemistry*, 14(6): 951–957.

Zhao H T, Nagy K L, Waples J S, Vance G F, 2000. Surfactant-templated mesoporous silicate materials as sorbents for organic pollutants in water. *Environmental Science & Technology*, 34(22): 4822–4827.